Journal of Power Sources 196 (2011) 1738–1743

Contents lists available at ScienceDirect

Journal of Power Sources

journal homepage: www.elsevier.com/locate/jpowsour

Sr_2CoMoO_6 anode for solid oxide fuel cell running on H_2 and CH_4 fuels

Ping Zhang[a,b], Yun-Hui Huang[b,c,*], Jin-Guang Cheng[b], Zong-Qiang Mao[d], John B. Goodenough[b]

[a] Engineering Research Center of Nano-GEO Materials of Education Ministry, China University of Geosciences, Wuhan 430074, China
[b] Texas Materials Institute, ETC 9.102, The University of Texas at Austin, Austin, TX 78712, USA
[c] State Key Laboratory of Materials Processing and Die and Mould Technology, School of Materials Science and Engineering, Huazhong University of Science and Technology, 1037 Luoyu Road, Wuhan 430074, China
[d] Institute of Nuclear and New Energy Technology, Tsinghua University, Beijing 100084, China

ARTICLE INFO

Article history:
Received 13 July 2010
Received in revised form 3 October 2010
Accepted 4 October 2010
Available online 8 October 2010

Keywords:
Solid oxide fuel cell
Double perovskite
Anode
Mixed ionic/electronic conductor
Methane oxidation reaction

ABSTRACT

The double perovskite $Sr_2CoMoO_{6-\delta}$ was investigated as a candidate anode for a solid oxide fuel cell (SOFC). Thermogravimetric analysis (TGA) and powder X-ray diffraction (XRD) showed that the cation array is retained to 800 °C in H_2 atmosphere with the introduction of a limited concentration of oxide–ion vacancies. Stoichiometric Sr_2CoMoO_6 has an antiferromagnetic Néel temperature $T_N \approx 37$ K, but after reduction in H_2 at 800 °C for 10 h, long-range magnetic order appears to set in above 300 K. In H_2, the electronic conductivity increases sharply with temperature in the interval 400 °C < T < 500 °C due to the onset of a loss of oxygen to make $Sr_2CoMoO_{6-\delta}$ a good mixed oxide–ion/electronic conductor (MIEC). With a 300-μm-thick $La_{0.8}Sr_{0.12}Ga_{0.83}Mg_{0.17}O_{2.815}$ (LSGM) as oxide–ion electrolyte and $SrCo_{0.8}Fe_{0.2}O_{3-\delta}$ as the cathode, the $Sr_2CoMoO_{6-\delta}$ anode gave a maximum power density of 1017 mW cm^{-2} in H_2 and 634 mW cm^{-2} in wet CH_4. A degradation of power in CH_4 was observed, which could be attributed to coke build up observed by energy dispersive spectroscopy (EDS).

1. Introduction

The solid oxide fuel cell (SOFC) with a solid oxide–ion conductor as electrolyte is a device for electrochemically converting the chemical energy of fuels to electric energy. Although the SOFC operates at a high temperature, it shows potential applications in both stationary and mobile generation of electric energy since it promises cleaner, more efficient energy conversion than either a conventional power plant or lower-temperature polymer-based fuel cells [1–2]. Early researches and demonstrations have shown that the SOFC/gas turbine (GT) hybrid system can offer net energy conversion efficiency as high as 70% [3–5]. The conventional SOFC with $Y_{2x}Zr_{1-2x}O_{2-x}$ (YSZ) as the electrolyte and a porous Ni-YSZ cermet as anode is commercially viable with pure H_2 or syngas as the fuel; but this anode is fouled by coke deposition and sulfur poisoning when operated on natural gas [6–9]. To resolve the anodic problem, the conventional strategy is to use purified fuel or to append a reformer of natural gas to H_2 and CO before it reaches the NiO/electrolyte composite anode. Although this strategy is efficient to avoid coking and sulfur poisoning, it brings an extra burden to the SOFC [10–13]. Therefore, development of alternative anode materials that can operate on natural gas would provide a cheaper, more convenient SOFC. For this purpose, oxides that are mixed oxide–ion/electron conductors (MIECs) in the reducing atmosphere have been under investigation [14–16].

Early experiments by Gorte and his co-workers demonstrated that copper composites with ceria or YSZ could be used as the anode materials for direct utilization of hydrocarbon fuels in a SOFC [17–18]. This material showed a good tolerance to H_2S at a fixed potential of 0.65 V, but its catalytic activity for hydrocarbon fuel proved to be disappointing [19]. Nevertheless, the ability of rare-earth doped ceria (RDC) to replenish O^{2-} ions to its surface to prevent coke build-up was an important point of reference for subsequent research. The next logical step was to develop other oxides that have not only a mixed ionic and electronic conductivity in the reducing anodic atmosphere but also a catalytic activity for the oxidation of hydrocarbons. The $ABO_{3-\delta}$ perovskite with a transition-metal B atom in the octahedral sites and a combination of rare-earth and alkaline-earth metals in the larger A sites is an attractive option. The earlier results of Tao et al. [8,9] indicated that the oxygen-deficient perovskite $(La_{0.75}Sr_{0.25})_{0.9}Cr_{0.5}Mn_{0.5}O_{3-\delta}$ with a mixed ion/electron conductivity (MIEC) gives a performance in H_2 fuel comparable to that of a Ni-based cermet anode and also an acceptable catalytic activity for the oxidation of CH_4 at high temperatures. In addition, these perovskite oxides have a thermal-expansion similar to that of the $La_{0.8}Sr_{0.2}Ga_{0.83}Mg_{0.17}O_{2.815}$ (LSGM)

* Corresponding author at: State Key Laboratory of Materials Processing and Die and Mould Technology, School of Materials Science and Engineering, Huazhong University of Science and Technology, 1037 Luoyu Road, Wuhan 430074, China. Tel.: +86 27 87558241; fax: +86 27 87558241.
E-mail addresses: huangyh@mail.hust.edu.cn, yunhuihuang@yahoo.com (Y.-H. Huang).

0378-7753/$ – see front matter © 2010 Elsevier B.V. All rights reserved.
doi:10.1016/j.jpowsour.2010.10.007

O^{2-}-ion electrolyte. However, the long-term performance of this anode is unsatisfactory due to poisoning by sulfur impurities and loss of electronic conductivity in the reducing atmosphere [20]. Even so, these studies pioneered the use of an oxygen-deficient perovskite with the anode of a SOFC.

Based on the ability of Mo(VI) and Mo(V) to form molybdyl ions allowing a sixfold-coordinated Mo(VI) to accept an electron while losing an oxide ligand, which is the basis of the $(PMo_{12}O_{40})^{3-}$ Keggin ion to partially oxidize acrolein to acrylic acid [21–23], we considered that it is feasible to use the Mo(VI)/Mo(V) couple as a catalytic agent for the anode of a SOFC. But the use of the Mo(VI)/Mo(V) couple as the catalytic agent requires a double perovskite with an M(II) partner ion to balance the charge. If the two alternating $BO_{6/2}$ and $B'O_{6/2}$ corner-shared octahedral-site cations are each stable in the case of less than sixfold oxygen coordination, the double perovskite structure can remain stable on the partial removal of oxygen. In our previous researches, we have explored $Sr_2MgMoO_{6-\delta}$ as an anode running on H_2 and CH_4; the Mg(II) ion is stable in either fourfold or sixfold oxygen coordination. In those experiments, a supporting 300-μm-thick LSGM plate with a thin $La_{0.4}Ce_{0.6}O_2$ (LDC) buffer layer was used as electrolyte; $SrCo_{0.8}Fe_{0.2}O_{3-\delta}$ (SCF) was the cathode. The fuel-cell system with $Sr_2MgMoO_{6-\delta}$ anode gave an excellent performance of P_{max} = 838 mW cm^{-2} in H_2 fuel at 800 °C. With dry CH_4 as the fuel, the P_{max} value reached 438mW cm^{-2} at the same operation temperature [24–25]. These results have prompted a study of other members of the Sr_2MMoO_6 family containing a 3*d*-block transition-metal M to investigate the role of the M cation. In Sr_2MgMoO_6, Mg ions are divalent; only the valence of Mo changes formally from +6 to +5 with the introduction of oxygen vacancies. The 3d-block transition-metal M ions are generally multivalent; the evolution of cation valence with oxygen-vacancy concentration in $Sr_2MMoO_{6-\delta}$ may be more complicated than that in Sr_2MgMoO_6. Moreover, the 3d-block transition metals, such as Co or Ni, commonly exhibit a catalytic activity for the oxidation of H_2 and CH_4. Therefore, we have systematically studied the valence states of M (M = Co or Ni) and Mo, the crystalline lattice parameters, the magnetic behavior and the oxygen-loss of the double perovskite $Sr_2MMoO_{6-\delta}$ in 5% H_2/Ar atmosphere; a preliminary study of the electrochemical performances of the double perovskite $Sr_2MMoO_{6-\delta}$ (M = Co or Ni) as anodes of a SOFC operating on dry and wet methane and on H_2 were also made [26]. In this paper, we report our recent results on the stability, conductivity, and magnetism of $Sr_2CoMoO_{6-\delta}$ in a reducing atmosphere at different temperatures, and the electrochemical performance of $Sr_2CoMoO_{6-\delta}$ as anodes in a SOFC running on H_2, as well as dry and wet methane.

2. Experimental

$Sr_2CoMoO_{6-\delta}$ (SCMO) was synthesized by solid-state reaction from stoichiometric proportions of $SrCO_3$, $CoCO_3$ (Alfa Aesar, 99%), and $(NH_4)_6Mo_7O_{24}{\cdot}4H_2O$ (Fisher Scientific, assay MoO_3, 81.5%). $SrCO_3$, $CoCO_3$ and $(NH_4)_6Mo_7O_{24}{\cdot}4H_2O$ were mixed and ground thoroughly in acetone medium until acetone volatilized fully. The powder was pelletized and calcined in air at 900 °C for 10 h. After cooling, the pellets were reground, re-pelletized, and calcined at 1300 °C for 10 h in air. This program was repeated several times to achieve a pure phase. The syntheses of the other compounds, $La_{0.8}Sr_{0.2}Ga_{0.83}Mg_{0.17}O_{2.815}$ (LSGM), $SrCo_{0.8}Fe_{0.2}O_{3-\delta}$ (SCF), and $La_{0.4}Ce_{0.6}O_{2-\delta}$ (LDC), has been described in detail elsewhere [25].

The phase purity of the samples was checked at room temperature by X-ray diffraction (XRD) with a Philips PW1830 diffractometer operating with Cu K_α radiation. The morphology was taken by a scanning electron microscope (SEM, Hitachi: S4500) and the elemental analysis with energy dispersive X-ray spectroscopy (EDS). The redox behavior was investigated by thermogravimetric analysis (TGA, Perkin-Elmer Pyris 1 and Netzsch STA 449 C) in a 5% H_2/Ar gas flow. The sample was heated from 50 °C to different terminal temperatures and then held for 2 h. The amount of sample powder was 30–45 mg and the heating/cooling rate was 2 °C min^{-1}. Measurement of magnetization was performed with a superconducting quantum interference device (Quantum Design: MPMS-XL5, SQUID). Resistance (R) was measured by a homemade dc four-probe setup in air, 5%H_2/Ar, pure H_2, dry and wet CH_4, respectively, over the temperature range of 673 K–1073 K. The sample was pressed into a rectangular bar and polished before sintering in air at 1250 °C for 24 h; Pt wire and Pt paste were used to make the four probes. During measurement, the oxygen partial pressure was monitored by a CG1000 oxygen analyzer (AMETEK/Thermox). The electrical resistivity (ρ) was calculated by $\rho = RS/l$, where S is the cross-sectional area and l is the length of the measured section of the rectangular bar. The conductivity (σ) was obtained by $\sigma = 1/\rho$.

A single test cell was fabricated by an electrolyte-supported technique. LSGM with a fixed thickness of 300 μm was used as the electrolyte with SCMO as the anode and SCF as the cathode [24,25]. Between the electrolyte and anode, a thin buffer layer of LDC was used to prevent interdiffusion of ionic species between the SCMO anode and the electrolyte [27–29]. LDC, SCMO and SCF powders were made into inks with a binder, V-006 (Heraeus). LDC ink was screen-printed onto one side of the LSGM disk followed by firing at 1300 °C in air for 1 h. SCMO was subsequently screen-printed onto the LDC layer and baked at 1250 °C in air for 1 h. SCF was finally screen-printed on the other side of the LSGM disk and sintered at 1100 °C in air for 1 h. The area of the working electrode was 0.24 cm^2 (0.6 cm × 0.4 cm). Pt gauze (Alfa Aesar, 52 mesh woven from 0.1 mm diameter wire, 99.9% metal basis) with a small amount of Pt paste (Heraeus) in separate dots was used as a current collector at both the anode and cathode sides for ensuring contact. A double-layer sealing design was applied in all single-cell tests. The assembled test cells were placed in the hot zone of a vertical furnace with air directly supplied to the cathode surface and the fuel to the anode surface at a flow rate of 30 mL min^{-1}. Before testing, the cells were exposed to 5% H_2/Ar for 20 h at 800 °C to reduce the SCMO and then purged with the fuel gas for 2 h. The performance measurements were typically carried out at 800 °C, and a constant potential was provided by an EG&G potentiostat/galvanostat model 273 running on a homemade LabView program. During a typical measurement, the cell voltage was varied from open-circuit voltage (OCV), which is around 1.2 V at 800 °C, to 0.2 V, and then back to OCV in a total of 30 steps and holding 10 s at each step.

3. Results and discussion

The XRD patterns of the Sr_2CoMoO_6 samples are shown in Fig. 1. The double-perovskite phase was obtained by just sintering in air. The superstructure peak (1 0 1) corresponds to the $CoO_{6/2}/MoO_{6/2}$ ordering. The splitting of the (0 0 4) and (2 2 0) reflections reflects a tetragonal distortion. A small quantity of $SrMoO_4$ impurity appears on the XRD patterns. The $SrMoO_4$ can be almost eliminated by being treated at 800 °C for 2 h in a flowing atmosphere of 5% H_2/Ar (see Fig. 1e).

Viola et al. [30] reported that reduced $Sr_2CoMoO_{6-\delta}$ can give rise to a limited number of oxygen vacancies and hence to some lower Mo oxidation states than Mo(VI). In our previous work, we also showed that some oxygen vacancies exist in the reduced $Sr_2CoMoO_{6-\delta}$ [26]. Here, we focus on the temperature dependence of the oxygen vacancies in the as-sintered Sr_2CoMoO_6 sample and the stability of the double-perovskite structure in 5% H_2/Ar, an atmosphere similar to that at the anode of an operating SOFC. In our experiments, the samples were heated in a flowing 5% H_2/Ar atmosphere to 750 °C, 800 °C, 850 °C and 900 °C, respectively, and then held for 2 h. Fig. 2 shows the recorded TGA curves. The weight

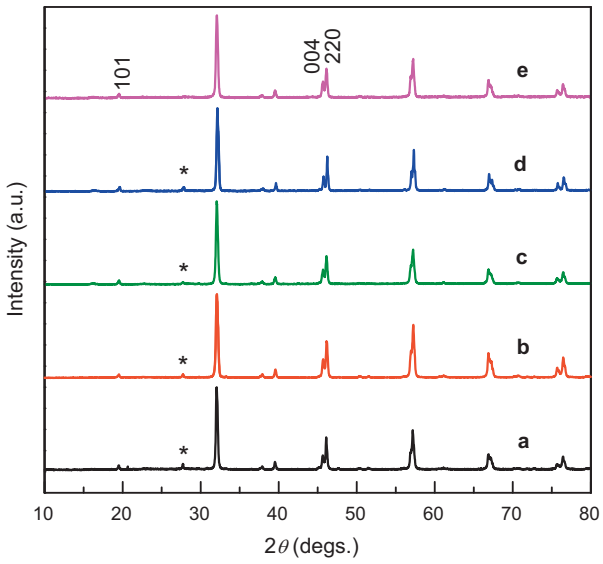

Fig. 1. XRD patterns for Sr_2CoMoO_6 sintered at 1300 °C in air for different hours: (a) 10 h, (b) 20 h, (c) 30 h, and (d) 40 h; (e) the sample (a) re-treated in 5% H_2/Ar for 2 h at 800 °C. The star (*) indicates the reflection peak of $SrMoO_4$ impurity phase.

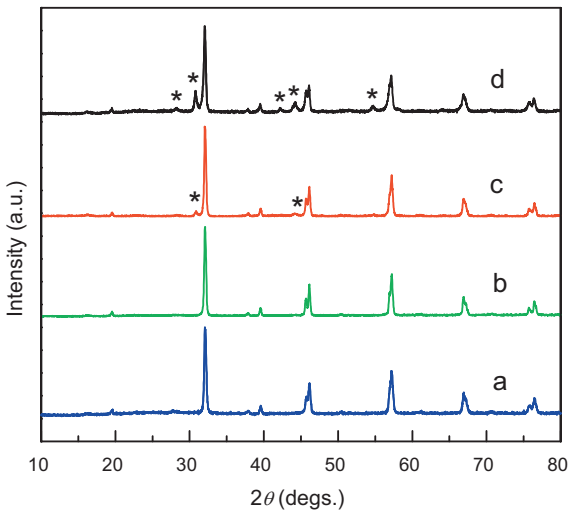

Fig. 3. XRD patterns for the $Sr_2CoMoO_{6-\delta}$ samples after TGA runs to different terminal temperatures (see Fig. 2): (a) 750 °C, (b) 800 °C, (c) 850 °C and (d) 900 °C. The stars refer to the reflection of the $SrMoO_4$ phase.

increases slightly at the initial stage, which may be ascribed to the absorption of a small amount of oxygen into the sample from the atmosphere. We take Fig. 2b as an example to demonstrate the thermogravimetric process. A weight loss of about 0.86% occurs on heating to 628 °C and 1.17% to 800° C, which corresponds to a $\delta = 0.23$ and 0.31 for $Sr_2CoMoO_{6-\delta}$ at 628 °C and 800 °C, respectively. When the sample was kept at 800 °C for 2 h, a further weight loss of 0.06% occurs. It can be clearly seen that the weight loss, i.e., the δ value, depends strongly on the terminal temperature. During the period when the sample was held at the different terminal temperatures for 2 h, the oxygen loss was 0.05%, 0.06%, 0.15% and 0.47%, respectively. Holding at higher temperature leads to a larger loss of oxygen.

XRD patterns for the above samples after the TGA runs are displayed in Fig. 3. With the terminal temperatures of 750 °C and 800 °C, no impurity phase was observed, which indicates that the sample is structurally stable. However, increasing the terminal temperature to 850 °C and 900 °C leads to the appearance of some $SrMoO_4$ phase. Since the Mo(VI)/Mo(V) redox couple is at a higher energy than the Co(III)/Co(II) couple, reduction of the sample first reduces any Co(III) to Co(II) and then reduces Mo(VI) to Mo(V). However, at temperature $T > 850$ °C, further oxygen loss leads to a disproportionation into Co and $SrMoO_4$. Therefore, Co(II)

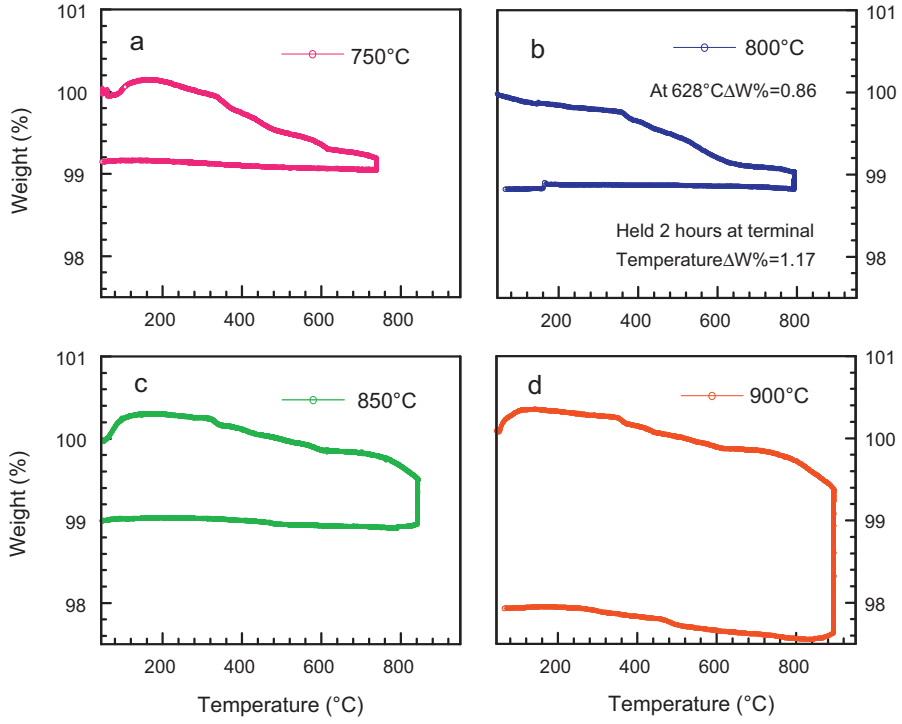

Fig. 2. TGA curves of $Sr_2CoMoO_{6-\delta}$ samples. The samples were heated to different terminal temperatures, held for 2 h, and then cooled down to room temperature in 5% H_2/Ar atmosphere with a heating rate 2 °C/min.

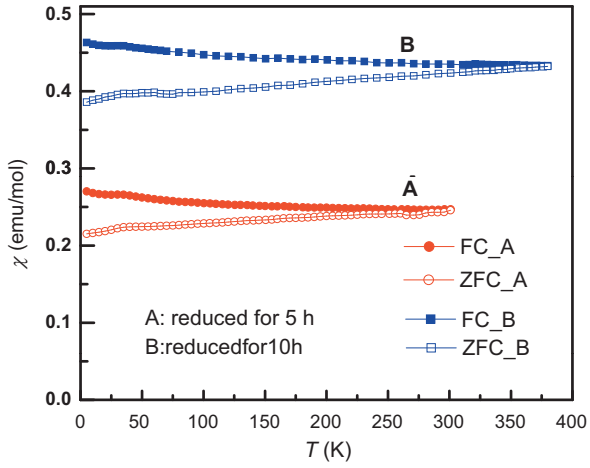

Fig. 4. Temperature dependence of the dc magnetic susceptibilities $\chi(T)$ measured under 1000 Oe with zero-field-cooling (ZFC) and field-cooling (FC) modes.

in the double perovskite $Sr_2CoMoO_{6-\delta}$ is stable and the loss of oxygen does not cause reduction of the Co(II) ion to Co provided the working temperature does not exceed 800 °C in an anode atmosphere.

The air-sintered Sr_2CoMoO_6 is an antiferromagnetic insulator with a Néel temperature T_N = 37 K. Similar results were reported in our previous work [26] and Ref. [30]. Here we further investigate the magnetic and electric behavior of this compound treated in pure H_2 atmosphere at 800 °C. Fig. 4 shows the temperature dependence of the dc magnetic susceptibilities $\chi(T)$ measured under a field of 1000 Oe with zero-field-cooling (ZFC) and field-cooling (FC) modes for $Sr_2CoMoO_{6-\delta}$ reduced under H_2 atmosphere at 800 °C for 5 h (sample A) and 10 h (sample B), respectively. The onset temperature of the splitting of the FC and ZFC curves increases with the loss of oxygen; the sample reduced in pure H_2 for 10 h exhibits a magnetic ordering near room temperature. Fig. 5 shows the field dependence of magnetization $M(H)$ at 5 K. The magnetization cannot be saturated even at a high field. The linear extrapolation of the high-field region to H = 0 yields a spontaneous magnetization of 0.09–0.18 μ_B/f.u., indicative of the existence of weak ferromagnetic components due to canting of an antiferromagnetic matrix.

The temperature dependence of the resistivity $\rho(T)$ and the linear plot of $\ln(\rho/T)$ vs T^{-1} of sample A are shown in Fig. 6. It exhibits a semiconductive behavior, which can be described roughly by a

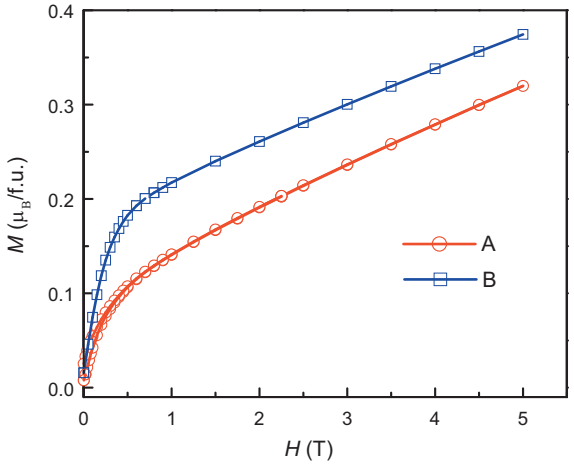

Fig. 5. Field dependence of magnetization $M(H)$ at 5 K for the reduced $Sr_2CoMoO_{6-\delta}$ samples.

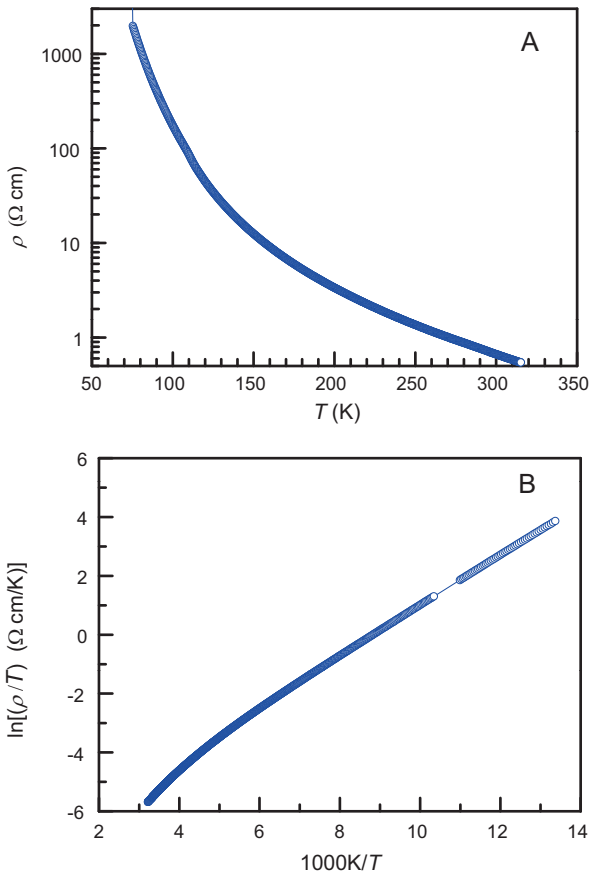

Fig. 6. (A) Temperature dependence of the resistivity $\rho(T)$ and (B) the plot of $\ln(\rho/T)$ vs. T^{-1} for $Sr_2CoMoO_{6-\delta}$ reduced in H_2 at 800 °C for 5 h.

small-polaron model, i.e., $\rho \sim T\exp(\Delta/kT)$ where Δ is an activation energy.

The curves shown in Fig. 7 are the conductivity data taken above 400 °C while heating respectively in air, 5% H_2/Ar, pure H_2, dry and wet CH_4 gas. In all atmospheres, the conductivity gives a positive temperature coefficient, i.e., the conductivity σ increases with temperature, which indicates that conduction is dominated by small polarons. In air, the temperature dependence of σ can be described over the whole temperature range 400 °C ≤ T ≤ 800 °C by the small-polaron expression $\sigma = (A/T)\exp(-E_a/kT)$, where the activation energy $E_a = \Delta H_m + (\Delta H_t/2)$ is the sum of the polaron motional enthalpy ΔH_m and the enthalpy ΔH_t to free a polaron from the oxygen vacancy that creates it. The Arrhenius plot $\log(\sigma T)$ vs. T^{-1} gives an $E_a = 0.134 \pm 0.001$ eV. In 5% H_2/Ar, reduction leads to the formation of oxygen vacancies with the introduction of additional electronic polaron charge carriers. The sharp increase in σ in the interval 400 °C < T < 500 °C occurs where the TGA curves of Fig. 2 show a step loss of oxygen, which means the increase in σ is due to an increase in the density of mobile polarons. A similar conductivity transition was observed in pure H_2, but in CH_4 the Arrhenius plots deviate from linear at a higher temperature in the case of dry CH_4 and over a broader temperature in wet CH_4.

Since the energy of the Co(III)/Co(II) redox couple lies below that of the Mo(VI)/Mo(V) couple, all the cobalt are Co(II) in the double perovskites $Sr_2CoMoO_{6-\delta}$, and the small-polaron charge carriers are Mo(V) moving in the Mo subarray. Based on balance of valence, the yield of Mo(V) is caused by the oxygen vacancies formed in reducing atmosphere. The temperature range of 400–600 °C for the oxygen loss in Fig. 2 is well consistent with that for the sharp σ increase in Fig. 7. From Fig. 7A, we can see that ρ is almost the

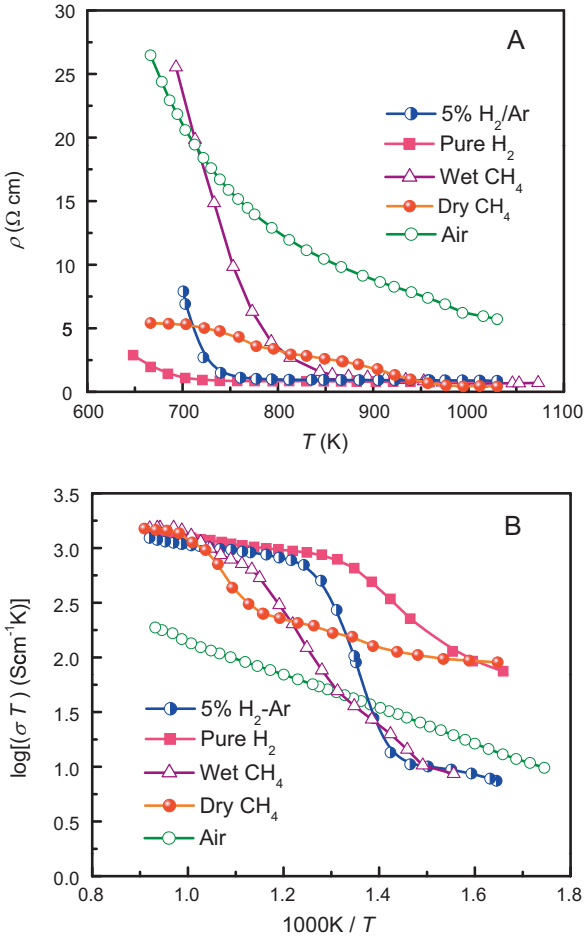

Fig. 7. (A) Temperature dependence of resistivity $\rho(T)$ and (B) Arrhenius plots of $\ln(\sigma/T)$ vs. T^{-1} for $Sr_2CoMoO_{6-\delta}$ in 5% H_2/Ar, pure H_2, dry CH_4 and wet CH_4.

lowest in H_2 atmosphere in the whole temperature range, and ρ in wet CH_4 becomes lower than that in dry CH_4 above 500 °C. According to the TGA curves, the oxygen vacancies can be formed if temperature is higher than 400 °C. In the lattice, oxygen ions are mobile through the vacancies, and the conductivity strongly depends on the oxygen vacancy. Therefore, $Sr_2CoMoO_{6-\delta}$ is mixed electronic/ionic conductor in H_2 and wet CH_4 at high temperature; in dry CH_4, the electronic/ionic conductivity may be poor due to the low conductivity.

The $Sr_2CoMoO_{6-\delta}$ sample was tested as the anode in a single fuel cell running on H_2 and CH_4 fuels to evaluate its electrochemical performance. The testing cell was assembled with a 300-μm-thick LSGM electrolyte, a porous SFC cathode and a thin LDC buffer layer between the electrolyte and anode, SCMO/LDC/LSGM/SCF. Fig. 8 shows the cell voltage and power density as a function of current density at 800 °C. In H_2 and wet CH_4 (containing 3% H_2O), the $Sr_2CoMoO_{6-\delta}$ anode exhibits an excellent performance. The maximum power density P_{max} at 800 °C is as high as 1017 mW cm^{-2} at a current density of 1817 mW cm^{-2} in H_2, and 634 mW cm^{-2} at 1054 mA cm^{-2} in wet CH_4, both of which are significantly higher than those with a $Sr_2MgMoO_{6-\delta}$ anode [24]. P_{max} in dry CH_4 is 452 mW cm^{-2} in the first power cycle, but the electrochemical performance after long-term running is disappointing. P_{max} as a function of power cycle in H_2 and CH_4 fuels is displayed in Fig. 9. Each cycle was run from OCV (open circuit voltage) to 0.2 V, and then back to OCV, which took 20 min. A total of 50 cycles, i.e., about 1000 min, was carried out for each fuel gas. Power loss over 50 cycles in H_2 and wet CH_4 is 10% and 11%, respectively. The

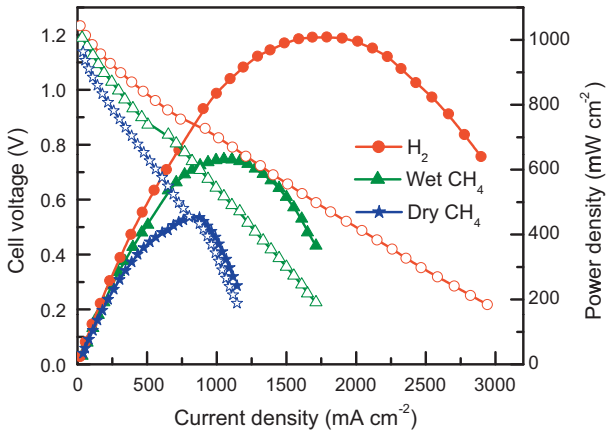

Fig. 8. Power density and cell voltage as functions of current density at 800 °C in H_2, dry CH_4 and wet CH_4 for $Sr_2CoMoO_{6-\delta}$.

power density in wet CH_4 is higher than that of $Sr_2MgMoO_{6-\delta}$ in our previous work [24]. In dry CH_4, the P_{max} value drops rapidly to 412.5 mW cm^{-2} after the 11th cycle and drops continuously down to 237.5 mW cm^{-2} after 50 cycles, showing a 53% power loss.

Fig. 10 shows the SEM image, the mapping of elemental C, and the pattern of EDS for the $Sr_2CoMoO_{6-\delta}$ anode after continuously running in H_2, wet and dry CH_4. A porous surface can be seen in Fig. 10A; at the same time, a clear coke deposition can also be observed from the mapping of carbon on the surface of the $Sr_2CoMoO_{6-\delta}$ anode, which may cause the rapid power loss with cycling in dry CH_4. Generally, the oxidation reaction of methane on the anode of a SOFC can be expressed as

$$CH_4 + 4O^{2-} = CO_2 + 2H_2O + 8e^- \quad (1)$$

In fact, the oxidation of methane to CO_2 is through a series of intermediate steps. For example, the reaction

$$CH_4 + 3O^{2-} = CO + 2H_2O + 6e^- \quad (2)$$

at an oxide-electrode surface is followed by (3) and the competing reaction (4)

$$CO + O^{2-} = CO_2 + 2e^- \quad (3)$$

$$2CO = C + CO_2 \quad (4)$$

Reaction (4) results in C–C bond formation. If reaction (3) is faster compared with reaction (4) on anoxide anode, the electrode

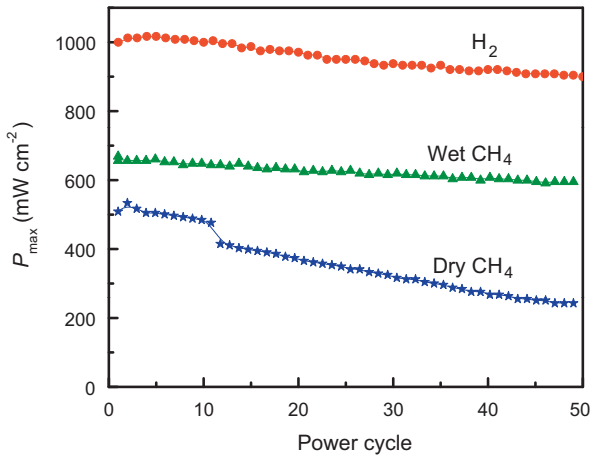

Fig. 9. Maximum power density as a function of power cycle for the $Sr_2CoMoO_{6-\delta}$ anode in H_2, dry and wet CH_4 fuels at 800 °C.

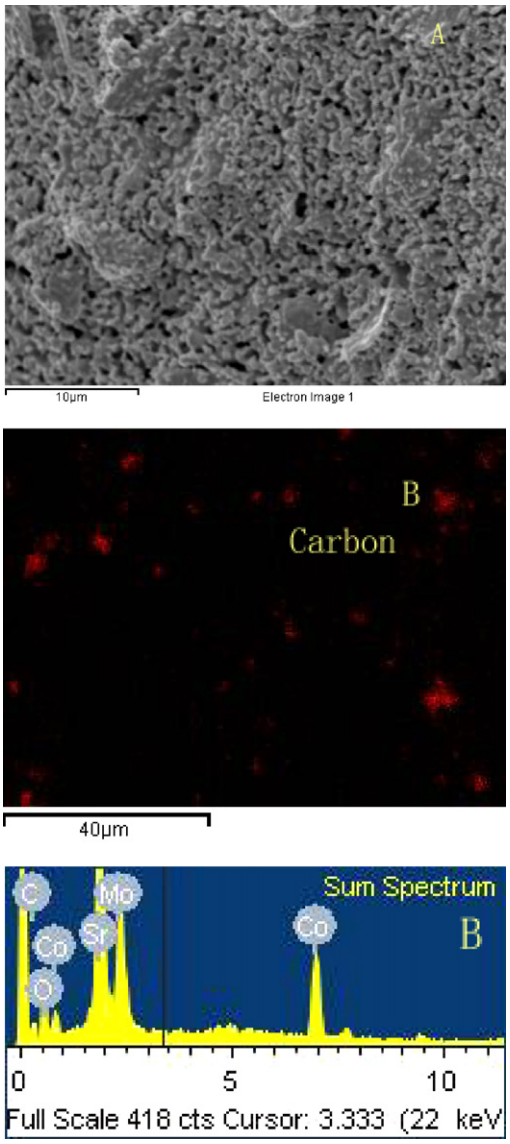

Fig. 10. (A) The SEM image, (B) the mapping of elemental C and the pattern of EDS of the $Sr_2CoMoO_{6-\delta}$ anode after continuously running in H_2, wet CH_4 and dry CH_4 for each 50 cycles.

surface may remain free of coke build-up. Removal of CO from the surface by adding steam to the feed gas, reaction (5), can be accompanied by (6):

$$CO + H_2O = CO_2 + H_2 \quad (5)$$

$$H_2 + O^{2-} = H_2O + 2e^- \quad (6)$$

Therefore, it is reasonable to propose that the high performance for $Sr_2CoMoO_{6-\delta}$ in wet CH_4 fuel is due to the reformer reaction (5) that not only removes the CO resulting from reaction (2) but also releases H_2 to create via reaction (6) the extra oxide–ion vacancies needed for good oxide–ion conductivity.

4. Conclusions

TGA and XRD data have shown that in pure H_2 atmosphere, the double perovskite $Sr_2CoMoO_{6-\delta}$ loses a limited amount of oxygen while retaining the double-perovskite cation structure up to 800 °C. In the interval 400 °C < T < 500 °C, the conductivity data show a sharp increase in the number of electronic charge carriers consistent with an increase in oxide–ion vacancies and therefore a higher oxide–ion conductivity. The electronic charge carriers are dielectric small polarons corresponding to mobile Mo(V) on a Mo subarray of primarily Mo(VI). Dry CH_4 removes oxygen from $Sr_2CoMoO_{6-\delta}$ only above 800 °C; in wet CH_4, the reformer reaction (5) removes CO from the surface as CO_2 and releases H_2 to extract oxygen from the oxide so that, at 800 °C, the oxide is a good MIEC anode for a SOFC. A maximum power density of 1017 mW cm^{-2} in H_2 and 634 mW cm^{-2} in wet CH_4 with a 300-μm-thick LGSM electrolyte was obtained at 800 °C. The high performance of $Sr_2CoMoO_{6-\delta}$ in wet CH_4 may be due to the creation of the extra oxide–ion vacancies needed for good oxide–ion conductivity during steam reforming of methane; but cycling in dry CH_4 gives a rapid degradation of power, which is probably the result of coke build-up due to reaction (4).

Acknowledgements

We thank the Robert A. Welch Foundation, Houston, TX, and the National Natural Science Foundation of China (Grant Nos. 50825203 and 20576129), for support of this work.

References

[1] N.Q. Minh, J. Am. Ceram. Soc. 76 (1993) 563–588.
[2] Z.L. Zhan, S.A. Barnett, Science 308 (2005) 844–847.
[3] S.C. Singhal, Solid State Ionics 135 (2000) 305–313.
[4] M.C. Williams, J.P. Strakey, W.A. Surdoval, J. Power Sources 143 (2005) 191–196.
[5] Department of Energy U.S., Fuel Cell Handbook, 7th ed. DOE, 2004.
[6] B.A. Boukamp, Nat. Mater. 2 (2003) 294–296.
[7] S. McIntosh, R.J. Gorte, Chem. Rev. 104 (2004) 4845.
[8] S.W. Tao, J.T.S. Irvine, Nat. Mater. 2 (2003) 320–323.
[9] S.W. Tao, J.T.S. Irvine, J. Electrochem. Soc. 151 (2004) A252–A259.
[10] B.C.H. Steele, I. Kelly, H. Middleton, R. Rudkin, Solid State Ionics 28–30 (1998) 1547–1552.
[11] A.L. Lee, R.F. Zabransky, W.J. Huber, Ind. Eng. Chem. Res. 29 (1990) 766–773.
[12] E.P. Murray, T. Tsai, S.A. Barnett, Nature 400 (1999) 649–651.
[13] Y. Matsuzaki, I. Yasuda, Solid State Ionics 132 (2000) 261–269.
[14] A. Atkinson, S. Barnett, R. Gorte, J.T.S. Irvine, et al., Nat. Mater. 3 (2004) 17–27.
[15] C.W. Sun, U. Stimming, J. Power Sources 171 (2007) 247–260.
[16] J.B. Goodenough, Y.H. Huang, J. Power Sources 173 (2007) 1–10.
[17] S. Park, J.M. Vohs, R.J. Gorte, Nature 404 (2000) 265–267.
[18] H. Kim, S. Park, J.M. Vohs, R.J. Gorte, J. Electrochem. Soc. 148 (2001) A693–A695.
[19] H.P. He, R.J. Gorte, J.M. Vohs, Electrochem. Solid-State Lett. 8 (2005) A279–A280.
[20] J. Wan, J.H. Zhu, J.B. Goodenough, Solid State Ionics 177 (2006) 1211–1217.
[21] J.B. Goodenough, Solid State Ionics 26 (1988) 87–100.
[22] J.B. Black, N.J. Clayden, P.L. Gai, J.D. Scott, E.M. Serwicka, J.B. Goodenough, J. Catal. 106 (1987) 1–15.
[23] J.B. Black, J.D. Scott, E.M. Serwicka, J.B. Goodenough, J. Catal. 106 (1987) 16–22.
[24] Y.H. Huang, R.I. Dass, Z.L. Xing, J.B. Goodenough, Science 312 (2006) 254–257.
[25] Y.H. Huang, R.I. Dass, J.C. Denyszyn, J.B. Goodenough, J. Electrochem. Soc. 153 (2006) A1266–A1272.
[26] Y.H. Huang, G. Liang, M. Croft, M. Lehtimäki, M. Karppinen, J.B. Goodenough, Chem. Mater. 21 (2009) 2319–2326.
[27] K.Q. Huang, J.B. Goodenough, J. Alloy Compd. 303–304 (2000) 454–464.
[28] K.Q. Huang, J.H. Wan, J.B. Goodenough, J. Electrochem. Soc. 148 (2001) A788–A794.
[29] J.H. Wan, J.Q. Yan, J.B. Goodenough, J. Electrochem. Soc. 152 (2005) A1511–A1515.
[30] M.C. Viola, M.J. Martínez-Lope, J.A. Alonso, P. Velasco, J.L. Martínez, J.C. Pedregosa, R.E. Carbonio, M.T. Fernández-Díaz, Chem. Mater. 14 (2002) 812–818.